Article:
Papadopoulou, E.L., Basnett, P., Paul, U.C. et al. (4 more authors) (2019) Green composites of poly(3-hydroxybutyrate) containing graphene nanoplatelets with desirable electrical conductivity and oxygen barrier properties. ACS Omega, 4 (22). pp. 19746-19755. ISSN 2470-1343

https://doi.org/10.1021/acsomega.9b02528

ACS OMEGA

Article

Cite This: ACS Omega 2019, 4, 19746−19755

http://pubs.acs.org/journal/acsodf

Green Composites of Poly(3-hydroxybutyrate) Containing Graphene Nanoplatelets with Desirable Electrical Conductivity and Oxygen Barrier Properties

Evie L. Papadopoulou,*[,†] Pooja Basnett,[§] Uttam C. Paul,[†] Sergio Marras,[‡] Luca Ceseracciu,[‡] Ipsita Roy,[§,∥] and Athanassia Athanassiou*[,†]

[†]Smart Materials and [‡]Materials Characterization Facility, Istituto Italiano di Tecnologia, via Morego 30, Genoa 16163, Italy

[§]Applied Biotechnology Research Group, School of Life Sciences, College of Liberal Arts and Sciences, University of Westminster, London W1W 6UW, U.K.

[∥]Department of Material Science and Engineering, Faculty of Engineering, University of Sheffield, Mappin Street, Sheffield S1 3JD, U.K.

Supporting Information

ABSTRACT: Poly(3-hydroxybutyrate), a green polymer originating from prokaryotic microbes, has been used to prepare composites with graphene nanoplatelets (GnP) at different concentrations. The films were fabricated by drop-casting and were hot-pressed at a temperature lower than their melting point to provide the molecular chains enough energy to reorientate while avoiding melting and degradation. It was found that hot-pressing increases crystallinity and improves mechanical properties. The Young's modulus increased from 1.2 to 1.6 GPa for the poly(3-hydroxybutyrate) (P(3HB)) films and from 0.5 to 2.2 GPa for the 15 wt % P(3HB)/GnP composites. Electrical resistivity decreases enormously with GnP concentration and hot-pressing, reaching 6 Ω sq^{-1} for the hot-pressed 30 wt % P(3HB)/GnP composite. Finally, the hot-pressed P(3HB) samples exhibit remarkable oxygen barrier properties, with oxygen permeability reaching 2800 mL μm m^{-2} day^{-1}, which becomes 895 mL μm m^{-2} day^{-1} when 15% GnP is added to the biopolymer matrix, one of the lowest values known for biopolymers and biocomposites. We propose that these biocomposites are used for elastic packaging and electronics.

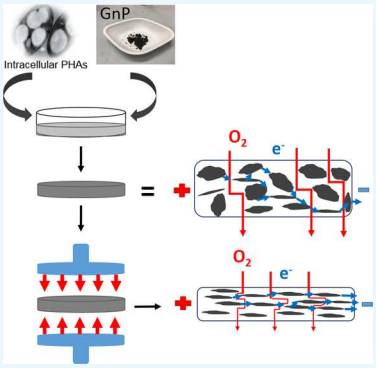

1. INTRODUCTION

The excessive use of plastics since the middle of the 20th century, in almost all sectors of everyday life, has resulted in enormous environmental pollution that now alarms scientists and society. Since 1964, plastic production has increased 20-fold, and it is expected to double again in 20 years and almost quadrupled by 2050 (World Economic Forum). In particular, in 2017, global plastic production reached 320 million tonnes, while the bioplastic production was only 2.05 million tonnes, about ∼1% of the plastics market.[1] Plastics are mainly derived from petroleum, the vast majority of these are not biodegradable, and the consequences of their extensive use include water pollution, bioaccumulation, and greenhouse effects.[2,3] Hence, the effort to substitute petroleum-based plastics with bioplastics, that come from natural resources and are biodegradable, has increased enormously in the last few years.[4−6]

A class of biomaterials that have attracted a lot of attention are the bio-based polyesters, namely polyhydroxyalkanoates (PHA).[7,8] PHAs are bioplastics produced completely by microorganisms,[9,10] and they are among the most versatile biodegradable polymers with properties very close to petroleum-based plastics.[11] The physical properties of PHAs, such as mechanical (i.e., Young's modulus), thermal (i.e., melting point), and their chemical properties, such as solvent solubility, largely depend on the microbial strain, the carbon source, and the method of extraction.[7,12] PHAs are categorized as medium-chain and short-chain length PHA, based on the number of carbon atoms in their monomer units, ranging from 4 to 14.[13] Recently, long-chain PHAs have also been reported with more than 14 carbon atoms in their monomer units.[14] One of the most commonly used PHA is poly(3-hydroxybutyrate), P(3HB), a short-chain length PHA containing 4 carbon atoms in its monomer unit. P(3HB) is a highly crystalline thermoplastic with high melting temperatures of 172−180 °C, that is stiff and brittle.[15,16] It has a Young's modulus of 3.5−4.0 GPa and an elongation at break less than 5%. Due to its biocompatibility and biodegradability, P(3HB) is also considered as a promising bioplastic in biomedical applications[10,17−21] and the packaging industry.[22−24]

To meliorate the properties of P(3HB), different fillers have been added into the polymer matrix, like bioglass and hydroxyapatite.[15,25−29] As seen in these reports, there is an inherent porosity in the P(3HB) films, which leads to a

Received: August 7, 2019
Accepted: October 30, 2019
Published: November 12, 2019

DOI: 10.1021/acsomega.9b02528
ACS Omega 2019, 4, 19746−19755

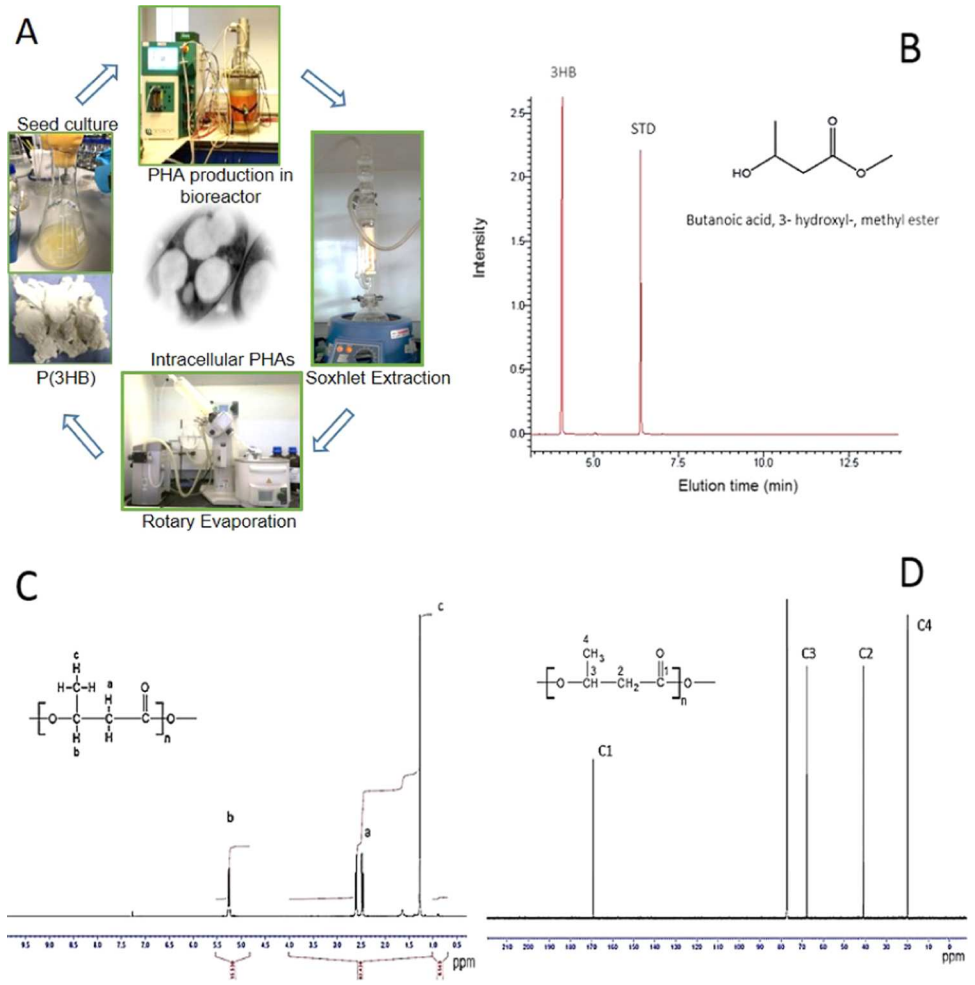

Figure 1. (A) Production and extraction of P(3HB) in a 15L bioreactor (Intracellular PHAs photo courtesy of Higuchi-Takeuchi et al., Copyright 2016[44]), (B) gas chromatography−mass spectrometry (GC−MS) spectra of P(3HB), (C) ^{1}H and (D) ^{13}C NMR spectra of P(3HB).

dependence on the mechanical properties of the composite on the size of the filler.[26] More specifically, while the stiffness of the matrix increases for fillers in the nanoscale size, the inverse occurs in the case of microsized fillers, allowing the possibility to tailor stiffness according to the application.

Graphene nanoplatelets (GnP) have been extensively used as reinforcing fillers in polymer matrices. They possess identical surface chemistry with carbon nanotubes, but they have a planar geometry, combining the laminar properties of layered silicates with the physical properties of graphene.[30] Hence, due to their special electrical and mechanical properties, lubricating planar surfaces, and flexibility, they are considered ideal for tailoring the properties of polymer matrices.[31,32] We thus consider GnP as an interesting filler for the P(3HB) polymer matrix, not only to enhance the mechanical properties of the matrix but, in addition, to convey electrical properties to an otherwise insulating material.

Good dispersion and interfacial interactions of the fillers in a polymer matrix are the main important parameters that need to be fulfilled when fillers are used as reinforcing agents in polymers. GnP have a poor affinity with most polymers, due to the inert chemical character of their surfaces, and their homogeneous distribution in the polymer matrices is still a challenge. The improvement in the dispersion of GnP in polymers has been addressed by different methods, like filler functionalization prior to mixing[33] or in situ polymerization in the presence of carbon nanotubes.[34] The aforementioned techniques are able to improve composite quality; however, they introduce time-consuming steps and/or highly specialized chemical procedures. Recently, uniaxial hot-pressing, as a post-treatment, has been used to improve composite performance, with respect to both electrical conductivity[35,36] and mechanical properties.[37] The enhanced performance is caused by the densification and alignment of the fillers. However, to the best of our knowledge, there is no previous study on the effect of hot-pressing on PHA composites.

In this work, we report for the first time, the effects of hot-pressing on the crystallinity, oxygen barrier, and the electrical and mechanical properties of P(3HB). P(3HB)-based films were produced by solution processing through simple casting, starting from P(3HB) solutions with or without the addition of GnP. Solution processing is a versatile method of polymer processing that can result in different polymer morphologies, like films[38,39] or fibers.[40,41] Solution processing for thin-film fabrication can be easily scaled up, using techniques for mass production like tape-casting and doctor blading.[42] After casting and solvent evaporation, the developed films were hot-pressed at a temperature slightly lower than the melting temperature of P(3HB), which increases the mobility of the polymer chains without degrading the polymer. Degradation is a common problem of thermally treated biopolyesters that undergo thermal processing methods, like extrusion or melt injection.[43]

DOI: 10.1021/acsomega.9b02528
ACS Omega 2019, 4, 19746−19755

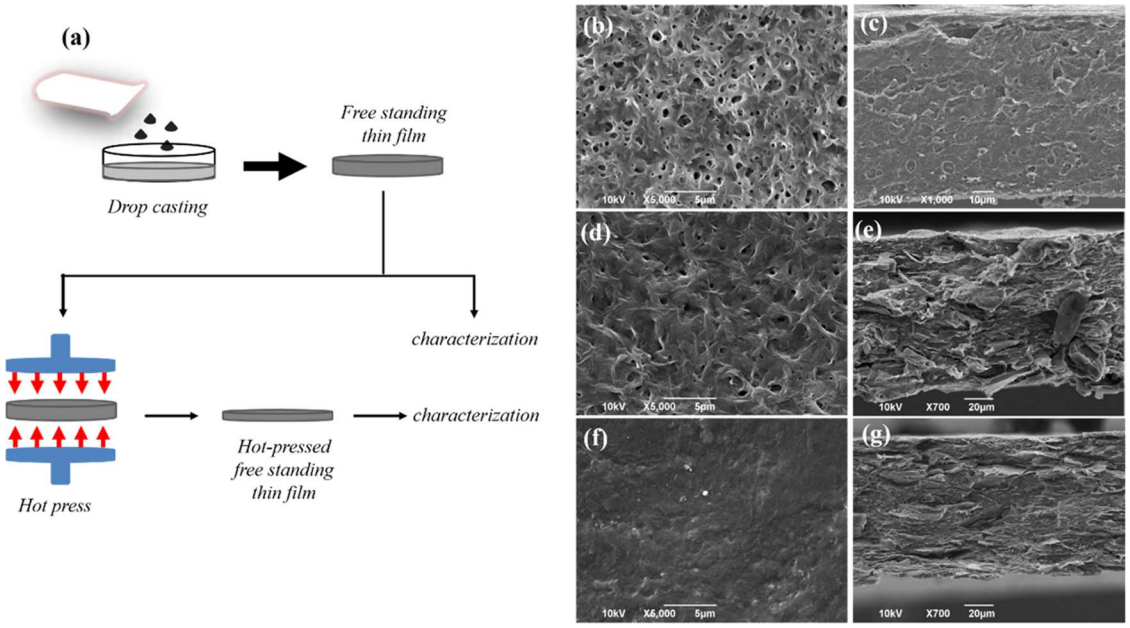

Figure 2. (a) Schematic diagram of the fabrication of the samples. Characteristic SEM images of (b) surface and (c) cross-section of the P(3HB) films, (d) surface and (e) cross-section of P(3HB)/10 wt % GnP composite films and (f) surface and (g) cross-section of the P(3HB)/10 wt % GnP composite films, after hot-pressing.

The crystallinity of the films was enhanced after hot-pressing, as measured using X-ray diffraction (XRD). In addition, mechanical properties were studied, and their behavior is discussed both as a result of GnP loading and hot-pressing, with the hot-pressed samples showing superior mechanical properties, since they were more elastic, regaining their original shape even after folding. Finally, the P(3HB) films were studied as potential candidates for two different applications, elastic packaging and electronics. For the packaging, the essential properties of the oxygen barrier were studied, and it was found that hot-pressing decreased the oxygen permeability (OP) of P(3HB) by more than 90%, making P(3HB) a very promising material for this specific application. Next, the electrical conductivity of the composites was studied with the increasing GnP concentration. For high GnP concentration and hot-pressing, the sheet resistance attained an unprecedented low value of 6 Ω sq^{-1}, making P(3HB) a highly valuable candidate for green flexible electronics.

2. RESULTS AND DISCUSSION

2.1. P(3HB) Extraction and Characterization. P(3HB) was produced by *Bacillus subtilis* OK2, using glucose as the carbon source, via batch fermentation, as shown in Figure 1A. The amount of biomass obtained at the end of fermentation was around 0.82 g L^{-1}. The final P(3HB) concentration was 0.24 g L^{-1}. The P(3HB) yield was 30% dry cell weight (dcw). As shown in Figure 1B, the monomeric composition of P(3HB) was confirmed using gas chromatography. The peak at 6.25 min represents the internal standard (methyl benzoate). The fragment peak at a retention time of 4.125 min represents butyric acid 3-hydroxy methyl ester, which confirmed that the polymer produced was indeed P(3HB).

Further structural characterization of the P(3HB) produced was carried out using NMR, as shown in Figure 1C for ^{1}H and Figure 1D for ^{13}C.

Analysis of the ^{1}H and ^{13}C NMR spectra is in agreement with the GC−MS spectra, hence confirming that the polymer produced by *B. subtilis* OK2 with glucose as the carbon source is P(3HB), as also identified by GC−MS. In addition to the chemical and structural properties, the thermal properties of P(3HB) were analyzed using differential scanning calorimetry (DSC) (Figure S1a).

2.2. Morphology of P(3HB)/GnP Composites. Figure 2a depicts the different steps of the fabrication method, which are described analytically in the Experimental Section. In brief, homogeneous dispersions of GnP at different concentrations in chloroform/P(3HB) solutions were drop-cast in glass Petri dishes. After solvent evaporation, very uniform, free-standing films were obtained, which were used either as prepared, or were subsequently hot-pressed. Representative scanning electron microscopy (SEM) images of P(3HB) and P(3HB)/10% GnP depict the surface and the cross-section of the respective samples. The surface of pure P(3HB) films present the typical rough and slightly porous structure of these types of polymers,[26] which are also seen in the cross-section, as shown in Figure 2b,c, respectively. When GnP are added in the P(3HB) matrix, the surface attains a similar porous morphology, and the GnP do not seem to be exposed on the surface of the polymer, as seen in Figure 2d. The cross-section of the P(3HB)/GnP sample, shown in Figure 2e, presents a dense P(3HB) matrix, with the GnP distributed quite homogeneously within it. Finally, after hot-pressing, the porous structure totally disappears, as seen in Figure 2f for P(3HB)/10% GnP, while the GnP are compacted and oriented parallel to the basal plane, in a brick-mortar-like structure (Figure 2g).

2.3. Crystallographic Investigation and Raman Studies. In Figure 3a, the XRD pattern of pure P(3HB), measured in the transmission mode, exhibits two intense peaks at 13.4 and 16.9° assigned to the (020) and (110) planes of the orthorhombic unit cell. Two more distinct peaks appear at 25.5 and 27.1° and are assigned to the (130) and (040) planes. In addition, the band at ∼22° is due to the broadening of the peaks corresponding to the (101) and (111) planes. Using the diffractograms presented in Figure 3a, the crystal structure of

DOI: 10.1021/acsomega.9b02528
ACS Omega 2019, 4, 19746−19755

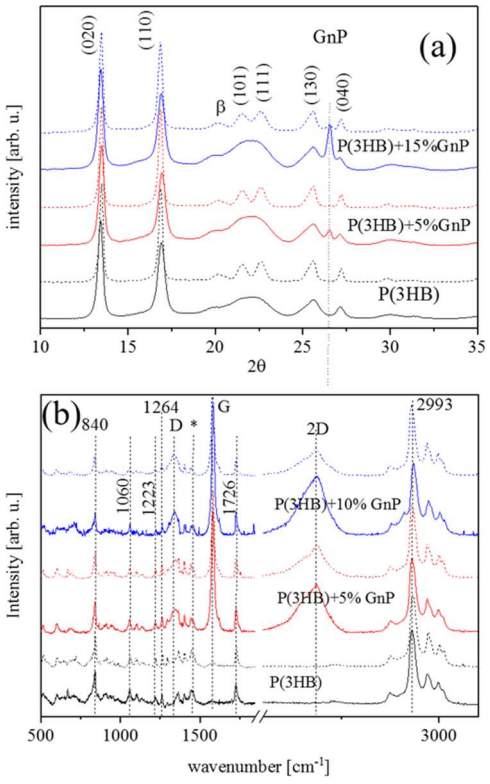

Figure 3. (a) XRD in the transmission mode of the P(3HB)/GnP composites, before (line) and after (dotted line) hot-pressing, (b) μRaman spectra for the P(3HB)/GnP composites before (solid line) and after (dotted line) hot-pressing. The asterisk (*) indicates the split band at 1445/1457 cm^{-1}.

the P(3HB) films was simulated using the crystallographic software Mercury CSD 3.9 from CCDC (Cambridge Crystallographic Data Center) and shows the characteristic helical chain conformation (α-form, shown in Figure S2 in the Supporting Information (SI)).

When GnP are added into the P(3HB) matrix, a new peak appears at approximately 26.55°, which corresponds to the (002) peak of graphite (ICSD collection code 76767), and therefore comes from the embedded GnP. The intensity of this peak increases as the concentration of GnP in the P(3HB) matrix increases, as expected.

Following hot-pressing, the XRD characterization was performed again in all of the samples. Comparing the diffractograms of the pristine and the hot-pressed P(3HB) samples, it is evident that the hot-pressed films are more crystalline: the (020) and (110) peaks are considerably narrow, for example, the full width at half-maximum of the (020) peak decreases from ca. 0.33 for pristine samples to ca. 0.23 for the hot-pressed ones. Furthermore, the broad band that was centered at ~22°, splits into two distinct peaks at 21.5 and 22.6°, assigned to (101) and (111) planes of the orthorhombic unit cell. Finally, after hot-pressing, a well-defined peak appears at ~20.1°, due to the presence of a small amount of β form crystals.[45] The β form of P(3HB) is related to the presence of a high level of molecular stretching in the amorphous region between the α-crystalline lamellae.[46]

For the composite samples, the GnP peak at 26.55° is greatly suppressed in the hot-pressed film, implying the increased orientation of the GnP basal planes along the plane of the film, i.e., perpendicular to the beam. Due to the transmission geometry of the beam in XRD, any planes perpendicular to the beam are not expected to give diffraction peaks. This is corroborated by the SEM images, as shown in Figure 2g, where the planar orientation of the GnP is evident. DSC measurements of the pristine and the hot-pressed P(3HB) films (Figure S1b in the SI) support the finding of higher crystallinity after hot-pressing and show an increase in the melting temperature of P(3HB) by approximately 20 °C. It is interesting to note here that, after hot-pressing, the P(3HB) films are no longer able to dissolve in chloroform, unlike the pristine ones. This might be due to the increase in crystallinity.[47,48]

Micro-Raman is a powerful, nondestructive characterization technique that has been extensively used to study both P(3HB) and graphene. Here, pure P(3HB) films and composites were studied by μRaman spectroscopy, both before and after hot-pressing, and the results are shown in Figure 3b. In the case of the samples before hot-pressing, the Raman spectrum of pure P(3HB) exhibits the main vibrational modes at 840, 1060, 1223, 1264, 1726 cm^{-1}, a split band at 1445/1457 cm^{-1}, and several peaks within the region 2800−3100 cm^{-1}.[49] The 840 cm^{-1} peak is assigned to C-COO stretching, and the 1060 cm^{-1} peak to C-CH_3 stretching, of the polymer backbone. The vibrational modes at 1223 and 1264 cm^{-1} are characteristic modes of the helical structure of crystalline P(3HB). Band splitting, like the one at 1445/1457 cm^{-1}, has been observed to occur in polymers with helical structures due to intermolecular interactions.[49,50] The modes seen between 2800 and 3100 cm^{-1} are due to C−H stretching from the methyl, methylene, and methene groups. Finally, the vibrational mode at 1726 cm^{-1} comes from the C═O stretching. In the case of the P(3HB)/GnP composites, the fingerprint peaks of GnP appear at approximately 1340 cm^{-1} (D peak), 1582 cm^{-1} (G peak), and 2686 cm^{-1} (2D peak). From the shape of the 2D peak, we can conclude that the GnP in the composite form multilayer stacks (~5 layers).[51]

The band at 1726 cm^{-1} is of particular interest because its deconvolution (seen in Figure S3 in the SI) reveals the presence of three peaks, at approximately 1726, 1733, and 1744 cm^{-1}. The first two peaks are due to the crystalline phase of P(3HB), while the third one indicates the amorphous phase. By deconvoluting the ν(C═O) band to the 3 aforementioned peaks, for both P(3HB) and P(3HB) + 10 wt % GnP (Figure S3, in the SI), it is seen that in the presence of GnP, the peak assigned to the amorphous phase, at 1744 cm^{-1}, is highly suppressed, while the peak assigned to the crystalline phase, at 1726 cm^{-1}, increases in intensity. The ratio of the areas of the two peaks, A_{1726}/A_{1744}, is used to quantify the crystallinity of the samples. Indeed, this ratio increases with the addition of 10 wt % GnP, from 0.26 for pure P(3HB) to 2.79 for the P(3HB)/GnP composite (see Table 1 in the SI), indicating that the GnP result in an increase in the crystallinity of P(3HB), in agreement with previous studies.[39]

After hot-pressing, μRaman measurements were repeated, resulting in similar spectra as for the unpressed samples, as shown in Figure 3b. Here, the absence of a vibrational mode at 1658 cm^{-1}, which is a peak associated with the degradation of P(3HB),[49] indicates that there is no degradation taking place during the hot-pressing under the specific conditions used in this work. In addition, the change of the relative intensity of the band at 1445/1457 cm^{-1} (Figure S4 in the SI) indicates changes in the crystallinity of the polymer,[49] in agreement with the XRD and DSC analyses. Finally, the deconvolution of the ν(C═O) band, reveals a suppressed 1744 cm^{-1} peak, and

DOI: 10.1021/acsomega.9b02528
ACS Omega 2019, 4, 19746−19755

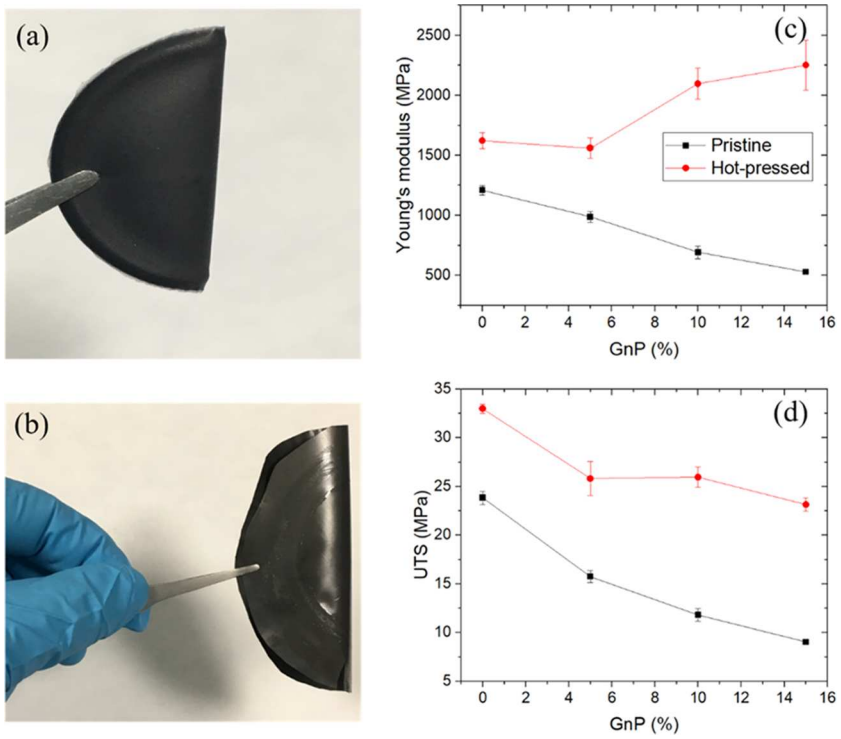

Figure 4. Photographs of folded P(3HB) composite films with 15 wt % GnP (a) pristine and (b) hot-pressed, (c) Young's modulus, and (d) ultimate tensile strength (UTS) of the nanocomposites as a function of the weight fraction of the GnP for pristine (black squares) and hot-pressed (red circles) films.

increased A_{1726}/A_{1744} ratio, due to the enhanced crystallinity after hot-pressing, for both pure P(3HB) and the P(3HB)/GnP composite (see Table 1 in the SI).

2.4. Mechanical Properties. The macroscopic appearance of the pristine and hot-pressed P(3HB)/GnP composites is shown in Figure 4a,b, where it can be seen that they are flexible enough to sustain folding, even at 180°. Nevertheless, the ductile character of the samples is enhanced after hot-pressing, since in this case, the samples can undergo multiple folding and unfolding, without any deformation and without the formation of cracks.

From the resulting stress−strain curves (shown in Figure S5 in the SI), as measured by static mechanical tests, the Young's modulus, ultimate tensile strength (UTS), and elongation at break were calculated and shown in Figure 4c,d. For the films before hot-pressing, embedding GnP results in a general reduction in the mechanical parameters. In particular, the Young's modulus of pure P(3HB) is ca. 1.2 GPa, in agreement with other reports,[25,26] decrease to ca. 0.5 GPa for 15 wt % GnP, resulting in a reduction of about 55%. Likewise, the UTS also suffers from a reduction of approximately 60% when 15 wt % of GnP is added to the P(3HB) matrix (Figure 4d). Finally, elongation at break (results not shown) decreases from 10 to 3% upon the addition of 15% GnP. Such a general reduction of the mechanical properties suggests a weak interaction between the polymer matrix and the reinforcing filler so that the particles do not participate in the load-bearing function. Instead, the filler particles act more like hollow zones within the matrix that can be starting points of failure upon stress. Consequently, both the stiffness and the strength are governed by the reduced matrix.

On the other hand, hot-pressing of the films results in enhanced stiffness of the P(3HB) matrix. The Young's modulus of the P(3HB) film increased from 1.2 to 1.6 GPa after hot-pressing, and it increases further with increasing GnP concentration reaching 2.2 GPa for 15 wt % GnP. This enhancement of the stiffness of approximately 40%, after hot-pressing, has also been observed for other polyester matrices, like polylactic acid (PLA),[37] and is attributed to the reorientation of the polymer chains during hot-pressing, at temperatures higher than the melting temperature. However, in the present case, hot-pressing was performed at a temperature lower than the melting point of the P(3HB) matrix, and therefore we expect less chain mobility and reorientation of the polymer chains. In addition, the elimination of the porosity that is present in the pristine films, as seen in Figure 2, helps to further enhance the stiffness of the films. Eliminating the porosity most likely also results in a better physical contact between the GnP and the matrix, improving the load transfer from the matrix, thus leading to a higher Young's modulus in all composites. This is also supported by the increase of the UTS after hot-pressing. In addition, it is known that the stiffness enhancement can be achieved by aligning the 2D fillers.[37] Indeed, as shown in the SEM picture of the hot-pressed composite in Figure 2g, a brick-and-mortar structure of the GnP is formed after hot-pressing. Furthermore, this result is supported by XRD, where the GnP peak is greatly reduced after hot-pressing, due to the parallel orientation of the GnP.

Furthermore, for low GnP concentrations, the presence of GnP can create spots of intensified stress, which can induce the onset of cracks, resulting in early fracture. For the GnP concentration higher than 5%, the percolation threshold appears (also discussed in paragraph 3.5) and the GnP form continuous chains, shunting the stress from the polymer matrix, and the Young's modulus follows an almost linear increase[52] while UTS stabilizes at a constant value. At the same time, the

DOI: 10.1021/acsomega.9b02528
ACS Omega 2019, 4, 19746−19755

UTS decreases with the increasing GnP concentration, even after hot-pressing, especially for low GnP concentrations. At low GnP concentrations, GnP are not continuous even after hot-pressing; hence, at large deformation, they lose the capability to bear the load, while the stress reaches the failure value within the matrix.

Finally, although elongation at break decreases from ca. 10% to ca. 3% with GnP addition, and this behavior does not alter after hot-pressing, however, the films remain flexible enough after hot-pressing, as shown in Figure 4b, and they can be easily handled, facilitating their use in all possible applications.

2.5. Electrical Properties. Electronic waste is becoming an increasing menace in our current times. As the lifetime of electronic devices is getting shorter every year, electronic waste reached 44.7 million tons in 2016 (United Nations), posing a growing danger for the environment. This problem is addressed by the emerging area of research of biomaterials that can be used in electronics, where the tendency is to substitute rigid materials with organic, flexible, and biodegradable polymers.[53] To the best of our knowledge, there is only one study that proposes P(3HB) as a conductive material when reinforced with carbon nanotubes.[54] Here, we have studied for the first time the electrical properties of the P(3HB) composites as a function of GnP concentration, and the results are presented in Figure 5. Even though P(3HB) is an insulator, with a sheet resistance of > 10^{10} Ω sq^{-1}, when GnP are added in the matrix, the resistance becomes lower, exhibiting an abrupt decrease from 10^{10} to 10^{5} Ω sq^{-1}, at ∼7 wt % GnP, in agreement with the literature.[39,55] For GnP concentration higher than 15 wt %, the resistance saturates at approximately 150 Ω sq^{-1}.

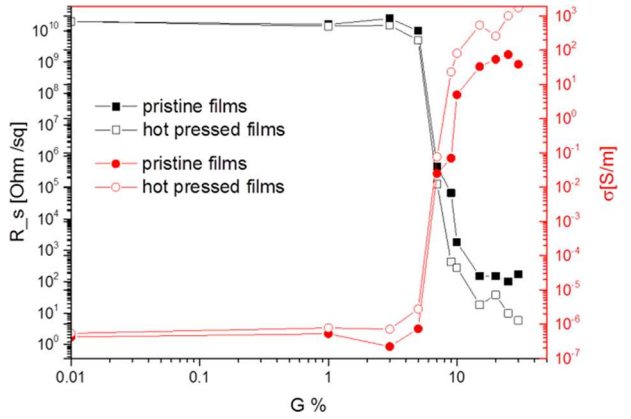

Figure 5. Sheet resistance (left-hand *Y*-axis) and electrical conductivity (right-hand *Y*-axis) as a function of GnP concentration, for composites both prior (closed symbols) and after hot-pressing (open symbols) (standard deviation shown in Figure S6).

The hot-pressed samples exhibit the same behavior, but their sheet resistance attains lower values than the pristine samples. The percolation threshold is the same for both pristine and hot-pressed samples, at ∼7 wt % GnP, where the resistivity is 5 orders of magnitude lower than that of pure P(3HB). However, at 5 wt % GnP, the sheet resistance of the hot-pressed samples is half an order of magnitude lower (1×10^{10} Ω sq^{-1} for unpressed sample, versus 5×10^{9} Ω sq^{-1} for the hot-pressed sample), while this difference augments with the increasing GnP concentration. For the GnP content higher than 15 wt %, the sheet resistance is lower than 20 Ω sq^{-1}, reaching approximately 6 Ω sq^{-1} for 30 wt % GnP, a value that was also measured in films of pure GnP.[55] On the right axis of Figure 5, the electrical conductivity is shown, as calculated from the sheet resistance. The excellent electrical properties of the composite are an added value, opening up possibilities for the use of 100% biodegradable and biocompatible materials in green and flexible electronics, to name a few applications. It is interesting to note here that the percolation threshold implies a continuous GnP network that shunts the weight load from the polymer matrix resulting in changes in the mechanical properties, as discussed in paragraph 3.4.

2.6. Oxygen Barrier Properties. Packaging is the largest application of plastics, representing 26% of their total volume and about half of this is related to food.[56] Hence, the necessity for green and biodegradable materials that can be used in packaging is increasing with the increase in the use of plastics.

PHAs have been investigated as a possible candidate for packaging applications[57,58] as a green alternative to more commonly used plastics, like the natural polylactic acid,[59] or the synthetic low-density polyethylene (LDPE) and polyethylene terephthalate (PET). Here, we have investigated the oxygen permeability (OP) of P(3HB), before and after hot-pressing, as calculated from the oxygen transmission rate (OTR) and the results are presented in Figure 6.

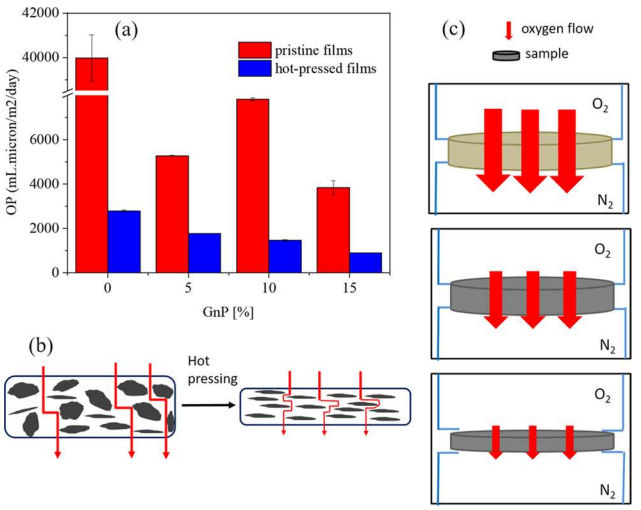

Figure 6. (a) Oxygen permeability values for pristine and hot-pressed P(3HB) films for GnP concentrations 0−15 wt %, (b) schematic representation of the action of GnP to the oxygen permeability in pristine and hot-pressed composites, and (c) simplified schematic representation of oxygen permeability for P(3HB) films (top panel), composites (middle panel), and hot-pressed samples (bottom panel).

As we see in Figure 6a, the OP of pristine P(3HB) is ca. 40 000 mL μm m^{-2} day^{-1}, and it decreases remarkably to a value as low as 2800 mL μm m^{-2} day^{-1}, after hot-pressing. This significant decrease (93%) of OP can be attributed to the synergistic effect of the collapse of the inherent porosity of the P(3HB) films and the increase of the P(3HB) crystallinity during hot-pressing, as demonstrated by X-ray diffraction and μRaman analysis. This induces higher tortuosity in the trajectory of the oxygen molecules, which inevitably reduces the oxygen permeability of the film.

Furthermore, polymer/GnP composites have been proposed not only for food packaging[60,61] but depending on their electrical properties, also for antistatic packaging for electronics.[62,63] However, data on oxygen barrier properties are

DOI: 10.1021/acsomega.9b02528
ACS Omega 2019, 4, 19746−19755

scarce in the literature.[64−66] Here, we have investigated the oxygen permeability behavior of the P(3HB)/GnP composites, also shown in Figure 6a. When GnP are added to the P(3HB) matrix, the oxygen permeability of the films suffers a significant reduction. Even 5 wt % addition of the GnP results in an OP of approximately 5300 mL μm m^{-2} day^{-1} (87% reduction), while for 15% GnP, the OP decreases further to 3800 mL μm m^{-2} day^{-1} (91% reduction). Hot-pressing results in even lower OP values, due to the increased crystallinity of the films and the loss of internal porosity, as explained above, obtaining a value as low as 895 mL μm m^{-2} day^{-1} for 15 wt % GnP. The inclusion of GnP in the P(3HB) matrix also results in higher tortuosity in the path of the oxygen molecules, which further increases by their alignment and compaction during hot-pressing, as shown schematically in Figure 6b.

It is interesting to compare these OP results with those obtained for other polymers currently used in food packaging applications, such as PLA, LDPE, and PET. The hot-pressed P(3HB) films exhibit lower oxygen permeability values than those obtained for LDPE (ca. 160 000 mL μm m^{-2} day^{-1}), and for PET (ca. 3000 mL μm m^{-2} day^{-1}).[67] Furthermore, the oxygen permeability values we obtain here are lower than the ones obtained for the copolymer poly-(3-hydroxybutyrate-*co*-3-hydroxyvalerate), or PHBV.[58] For the PHBV samples, oxygen permeability values were found to decrease for the lower 3-hydroxyvalerate content attaining a value of 8160 mL μm m^{-2} day^{-1} for 7 wt % 3-hydroxyvalerate concentration, decreasing further to 2590 mL μm m^{-2} day^{-1} with the addition of bacterial cellulose nanowhiskers. Even though the OP of pure PHBV is lower than the one we found for pristine P(3HB), the OP value we obtain after hot-pressing is much lower. Here, we should also note that although the reduction percentage after hot-pressing is similar for all composites, when we compare the composite films to the pristine P(3HB) one, the reduction in oxygen permeability reaches 98% (15 wt % GnP, hot-pressed sample), one of the highest reductions we know for graphene composites with polymers.[68] In Figure 6c, we show a simplified scheme to hypothesize the mechanism of reduction of OP in our samples, compared to the pristine P(3HB) films (upper panel). First, the inclusion of GnP results in the lower OP (middle panel), while hot-pressing further decreases the OP. These results indicate that the P(3HB) is indeed a very promising candidate for packaging applications, where a high barrier to oxygen is critical to avoid or reduce the oxidative degradation processes. Its oxygen permeability can be tuned, either by hot-pressing and/or with the inclusion of GnP, over a very broad range of values.

3. CONCLUSIONS

Biocomposites of P(3HB) and GnP were fabricated by a simple drop-cast method and were studied for their physical properties. Furthermore, the films were subjected to uniaxial hot-pressing, and their properties were compared to the pristine ones. The GnP disperse well in the P(3HB) matrix, and subsequent hot-pressing resulted in the collapse of the inherent porosity of P(3HB) films, while the GnP aligned parallel to the basal plane of the film, in a brick-and-mortar-like structure. In addition, after hot-pressing, the crystallinity of the films increased, as shown by XRD and μRaman measurements, while the improved interaction between the polymer matrix and the filler was reflected in the enhanced Young's modulus of the films with increasing GnP concentrations. A detailed study of the electrical properties showed the dependence of electrical conductivity of the P(3HB) films on the GnP concentration. As expected, the conductivity of the composites increased with the increasing GnP concentration, reaching approximately 100 S m^{-1}. In addition, after hot-pressing, even though there was no clear shift of the percolation threshold, a clear increase of the electrical conductivity was observed, which was attributed to the collapse of the inherent porosity and the improved interaction of the GnP with the P(3HB) matrix, with conductivity reaching a value as high as 1000 S m^{-1}. Finally, pure P(3HB) films were tested for oxygen barrier properties, and it was seen that oxygen permeability of the P(3HB) pristine film was improved by the inclusion of GnP fillers. Subsequent hot-pressing lead to an impressive decrease of the oxygen permeability of P(3HB) composite films by ca. 98%, making it one of the most promising biomaterials for oxygen barrier applications and packaging.

The fabrication method presented herein is a standard solution casting method adapted for small scale laboratory thin-film production. This process gives homogeneous films, but it is not suitable for films with a diameter bigger than 20−30 cm, and in addition, drying times can be too long. However, it is shown that solution processing can be scaled up using doctor blade or tape-casting techniques, producing large, uniform, composite films in just a few hours.[42]

We believe that the results presented here reveal, for the first time, the highly desirable properties of P(3HB)/GnP composites, especially the tuning of the electrical conductivity and the oxygen permeability. The aforementioned obtained properties combined with the possibility of the large scale production of the composite films through solution processing techniques, like doctor blading and subsequent hot-press, open completely new possibilities for the use of P(3HB), in two highly relevant and environmentally crucial technological fields, namely, packaging and green electronics.

4. EXPERIMENTAL SECTION

4.1. Production and Extraction of SCL-PHA, Poly(3-hydroxybutyrate), P(3HB). P(3HB) was produced by *B. subtilis* OK2 using glucose at a concentration of 35 g L^{-1} as the sole carbon substrate and under nitrogen limiting conditions. Bacterial fermentation was initiated by inoculating a sterile nutrient broth with a single colony of *B. subtilis* OK2. This was incubated for 16 h at 30 °C, 200 rpm. Ten percent (v/v) of the inoculum was used to inoculate the production stage (modified Kannan and Rehacek media), which was incubated at 30 °C, 200 rpm for 48 h. The temperature was controlled at 30 °C, the pH was set at 6.8, and 1 vvm air was supplied to the bioreactor. The pH and DOT were monitored throughout the course of the fermentation but not maintained. At the end of the fermentation, the biomass was obtained via centrifugation. The wet biomass was subjected to repeated washings with deionized water and homogenized (10 min in T25 basic homogenizer, IKA Labortechnik) to induce outer cell membrane disruption. The homogenized biomass was lyophilized in the preparation for polymer extraction.

PHA was extracted from the biomass using an optimized two-stage Soxhlet extraction method. Powdered biomass was added to the thimble, which was placed in the extractor. The cells were refluxed in methanol for 24−48 h to remove methanol soluble impurities, followed by chloroform for 48 h to extract the polymer. The polymer was precipitated in ice-cold methanol while stirring. The polymer mass fraction (% dcw) was calculated as a percentage of the cell dry mass.

DOI: 10.1021/acsomega.9b02528
ACS Omega 2019, 4, 19746−19755

4.2. Gas Chromatography (GC). Chemical characterization of the polymer was carried out using GC. Prior to GC analysis, polymer samples were methanolyzed. GC−MS analysis was carried out using a Varian GS system consisting of Chrompack CP-3800 gas chromatograph and the Saturn 200 MS/MS block.

4.3. NMR. Structural identification of the polymer was carried out using ^{13}C and ^{1}H NMR spectroscopy. Twenty milligrams of the purified polymer sample were dissolved in 1 mL of deuterated chloroform ($CDCl_3$) and analyzed. All NMR spectra were measured at 298 K. Solution ^{1}H and ^{13}C NMR spectra were recorded on a Bruker NMR spectrometer. Data acquisition and processing were performed using standard Bruker TopSpin (version 2.1) software. ^{1}H and ^{13}C chemical shifts were calibrated using the residual solvent peak (^{1}H 7.26 ppm, ^{13}C 77.15 ppm) for chloroform.

4.4. Differential Scanning Calorimetry (DSC). Thermal properties such as the melting temperature (T_m), glass transition temperature (T_g), and the crystallization temperature (T_c) of the PHA produced were determined using DSC. Five milligrams of the polymer sample were used for this analysis. Samples were heated, cooled, and then reheated between −50 and 100 °C at a heating rate of 20 °C min^{-1}. (ca. −5 °C) to assure the mobility to the polymer chains.[25]

4.5. Film Preparation. GnP (grade Ultra-G+) were provided by Directa Plus Spa (Italy). Their lateral dimension is a few tens of micrometers, while the thickness is a few tens of nanometers.[37] Chloroform was acquired from Sigma-Aldrich and used as received. To prepare the solutions for solvent cast films, P(3HB) was dissolved in chloroform at a 5 wt % concentration. After dissolution, GnP were added at concentrations ranging from 0 to 30 wt %. The solution was rendered homogeneous by bath sonication for 7 h at 59 Hz. Subsequently, the solutions were drop-cast on glass Petri dishes and covered to slow down the evaporation. The resulting films were free-standing and had a thickness of approximately 200 μm.

For the hot-pressed samples, the samples were pressed uniaxially (15 bar) for 30 min at a temperature of 150 °C. This temperature is lower than the melting temperature of P(3HB) (ca. 172 °C) and thus it is not expected to melt the samples, but higher than its glass transition temperature (<10 °C). During hot-pressing, the samples were placed between nonstick Teflon films (Advent Research Materials, Art. Num. FP823338) to prevent their sticking to the surfaces of the press. The hot-pressing was performed using a Specac-Atlas 15T Manual Hydraulic press. Film preparation and hot-pressing were carried out at ambient conditions.

4.6. Characterization of the Films. The morphology of the surface and the cross-section of the films were studied by scanning electron microscopy (SEM, JEOL JSM-6490LA).

X-ray diffraction measurements in a transmission geometry (TXRD) were performed using a Rigaku SmartLab X-ray powder diffractometer (a 9 kW Cu Kα rotating anode, operating at 40 kV and 150 mA) and a D\teX Ultra 1D silicon strip detector. A Göbel mirror was used to convert the divergent X-ray beam into a parallel beam and to suppress the Cu Kβ radiation. The analysis of the diffractograms was carried out using PDXL 2.7.2.0 software from Rigaku. A custom-made holder has been used for the thin film analysis performed in a transmission geometry (TXRD), which presents several advantages for thin-film studies. It avoids the presence of artifacts in the diffractograms, especially in the case of irregular and crinkled surfaces. In addition, the volume of the sample analyzed during each angular scan is constant in the transmission geometry, while the linear detector used in TXRD allows shorter measuring times. For the peak assignment, the reference structure 94-873-7695 from the Cambridge Structural Database (CSD) was used.[69]

Micro-Raman spectra were collected at ambiance by a Horiba Jobin Yvon LabRAM HR800 μRaman spectrometer, equipped with a microscope. We used the 632.8 nm excitation line in backscattering geometry through a 50 × objective lens. The power of the laser was ca. 0.25 mW. The grating used was 600 lines per mm with a spectral resolution of approximately 1 cm^{-1}.

Differential scanning calorimeter (DSC) measurements were performed by a Perkin-Elmer Diamond calorimeter, using an indium standard for the calibration. Initially, we measured the baseline from 0 °C up to 200 °C at a rate of 10 °C min^{-1}. Then, ca. 12 mg of the P(3HB) films were placed in aluminum sample pans, and heated from −5 to 200 °C at a rate of 10 °C min^{-1} and subsequently cooled down to 0 °C at a rate of 10 °C min^{-1}.

4.7. Electrical Properties of the Composite Films. The electrical transport properties of the P(3HB)/GnP nanocomposites were studied using a Karl Suss RA150 Probe Station, by the 2-probe method. Square pieces of the samples were cut and silver electrodes were applied at the opposite sides (2 mm apart). The bias ranged from −1 to + 1 V.

4.8. Mechanical Properties of the Composite Films. Mechanical properties were measured by uniaxial tension tests on an Instron 3365 Universal testing equipment. The samples were cut into 2 mm wide and 10 mm long strips and mounted on the clamps. The thickness was ca. 0.2 mm for pristine samples and ca. 0.1 mm for hot-pressed samples. The displacement rate was 1 mm min^{-1}. From the resulting stress−strain curves, the Young's modulus, ultimate tensile strength, and elongation at break were calculated. Average results were calculated from 3 repeats for each material.

4.9. Oxygen Barrier Properties of the Composite Films. The oxygen permeation tests of the composites were performed using an Oxysense 5250i device (Oxysense) equipped with a film permeation chamber, following the protocol presented in ref 38 (ASTM Method F3136-15). The cylindrical permeation chamber consists of two parts, the sensing well (purged with nitrogen) and the driving well (open). Square pieces of the samples (6 cm × 6 cm) were placed between the two wells. The monitor sensor on the sensing well, measured the oxygen transmission rate (OTR, mL m^{-2} day^{-1}), continuously until the steady state was reached, and the oxygen permeability (OP) of the films is then calculated by:

$$OP = OTR \times F_t$$

where F_t is the film thickness.

■ ASSOCIATED CONTENT

Supporting Information

The Supporting Information is available free of charge on the ACS Publications website at DOI: 10.1021/acsomega.9b02528.

DSC thermographs of raw polymer and composite films; the simulated crystal structure of P(3HB); curve fitting of the νC=O band (from the Raman spectra); the change of relative intensity of the split band at 1445/1457 cm^{-1} (from the Raman spectra); stress−strain curves; table

DOI: 10.1021/acsomega.9b02528
ACS Omega 2019, 4, 19746−19755

with ratios of the area of peaks associated with crystallinity (from Raman spectra) (PDF)

AUTHOR INFORMATION

Corresponding Authors

*E-mail: paraskevi.papadopoulou@iit.it. Tel +39 010 71781 705 (E.L.P.).

*E-mail: athanassia.athanassiou@iit.it. Tel: +39 010 71781 528 (A.A).

ORCID

Evie L. Papadopoulou: 0000-0001-5959-9730

Luca Ceseracciu: 0000-0003-3296-8051

Notes

The authors declare no competing financial interest.

ACKNOWLEDGMENTS

We would like to acknowledge Directa Plus S.p.a. (Italy) for kindly providing us with the graphene nanoplatelets. We would also like to acknowledge the ReBioStent project—the European Union's Seventh Program for research, technological development and demonstration under Grant agreement number 604251 and the Neurimp project under Grant Agreement No. 604450 for the funding provided to P.B.

REFERENCES

(1) https://www.european-bioplastics.org/wp-content/uploads/2016/02/Report_Bioplastics-Market-Data_2018.pdf.

(2) Lithner, D.; Larsson, Å.; Dave, G. Environmental and health hazard ranking and assessment of plastic polymers based on chemical composition. *Sci. Total Environ.* **2011**, *409*, 3309−3324.

(3) Mohanty, A. K.; Misra, M.; Hinrichsen, G. Biofibres, biodegradable polymers and biocomposites: An overview. *Macromol. Mater. Eng.* **2000**, *276*−*277*, 1−24.

(4) Chen, G.-Q.; Patel, M. K. Plastics Derived from Biological Sources: Present and Future: A Technical and Environmental Review. *Chem. Rev.* **2012**, *112*, 2082−2099.

(5) Ragauskas, A. J.; Williams, C. K.; Davison, B. H.; Britovsek, G.; Cairney, J.; Eckert, C. A.; Frederick, W. J.; Hallett, J. P.; Leak, D. J.; Liotta, C. L.; Mielenz, J. R.; Murphy, R.; Templer, R.; Tschaplinski, T. The Path Forward for Biofuels and Biomaterials. *Science* **2006**, *311*, 484−489.

(6) Perotto, G.; Ceseracciu, L.; Simonutti, R.; Paul, U. C.; Guzman-Puyol, S.; Tran, T.-N.; Bayer, I. S.; Athanassiou, A. Bioplastics from vegetable waste via an eco-friendly water-based process. *Green Chem.* **2018**, No. 11111.

(7) Keshavarz, T.; Roy, I. Polyhydroxyalkanoates: bioplastics with a green agenda. *Curr. Opin. Microbiol.* **2010**, *13*, 321−326.

(8) Kaur, G.; Roy, I. Strategies for large scale production of Polyhydroxyalkanoates. *Chem. Biochem. Eng. Q.* **2015**, *29*, 157−172.

(9) Zia, K. M.; Noreen, A.; Zuber, M.; Tabasum, S.; Mujahid, M. Recent developments and future prospects on bio-based polyesters derived from renewable resources: A review. *Int. J. Biol. Macromol.* **2016**, *82*, 1028−1040.

(10) Akaraonye, E.; Filip, J.; Safarikova, M.; Salih, V.; Keshavarz, T.; Knowles, J. C.; Roy, I. P(3HB) Based Magnetic Nanocomposites: Smart Materials for Bone Tissue Engineering. *J. Nanomater.* **2016**, *2016*, No. 14.

(11) Steinbüchel, A.; Füchtenbusch, B. Bacterial and other biological systems for polyester production. *Trends Biotechnol.* **1998**, *16*, 419−427.

(12) Lukasiewicz, B.; Basnett, P.; Nigmatullin, R.; Matharu, R.; Knowles, J. C.; Roy, I. Binary polyhydroxyalkanoate systems for soft tissue engineering. *Acta Biomater.* **2018**, *71*, 225−234.

(13) Basnett, P.; Marcello, E.; Lukasiewicz, B.; Panchal, B.; Nigmatullin, R.; Knowles, J. C.; Roy, I. Biosynthesis and characterization of a novel, biocompatible medium chain length polyhydroxyalkanoate by Pseudomonas mendocina CH50 using coconut oil as the carbon source. *J. Mater. Sci.: Mater. Med.* **2018**, *29*, No. 179.

(14) Koller, M. Chemical and Biochemical Engineering Approaches in Manufacturing Polyhydroxyalkanoate (PHA) Biopolyesters of Tailored Structure with Focus on the Diversity of Building Blocks. *Chem. Biochem. Eng. Q.* **2018**, *32*, 413−438.

(15) Misra, S. K.; Valappil, S. P.; Roy, I.; Boccaccini, A. R. Polyhydroxyalkanoate (PHA)/Inorganic Phase Composites for Tissue Engineering Applications. *Biomacromolecules* **2006**, *7*, 2249−2258.

(16) Akaraonye, E.; Moreno, C.; Knowles, J. C.; Keshavarz, T.; Roy, I. Poly(3-hydroxybutyrate) production by Bacillus cereus SPV using sugarcane molasses as the main carbon source. *Biotechnol. J.* **2012**, *7*, 293−303.

(17) Rai, R.; Keshavarz, T.; Roether, J. A.; Boccaccini, A. R.; Roy, I. Medium chain length polyhydroxyalkanoates, promising new biomedical materials for the future. *Mater. Sci. Eng., R* **2011**, *72*, 29−47.

(18) Hazer, D. B.; Kılıçay, E.; Hazer, B. Poly(3-hydroxyalkanoate)s: Diversification and biomedical applications: A state of the art review. *Mater. Sci. Eng., C* **2012**, *32*, 637−647.

(19) Lizarraga-Valderrama, L. R.; Nigmatullin, R.; Taylor, C.; Haycock, J. W.; Claeyssens, F.; Knowles, J. C.; Roy, I. Nerve tissue engineering using blends of poly(3-hydroxyalkanoates) for peripheral nerve regeneration. *Eng. Life Sci.* **2015**, *15*, 612−621.

(20) Yucel, D.; Kose, G. T.; Hasirci, V. Tissue Engineered, Guided Nerve Tube Consisting of Aligned Neural Stem Cells and Astrocytes. *Biomacromolecules* **2010**, *11*, 3584−3591.

(21) Bagdadi, A. V.; Safari, M.; Dubey, P.; Basnett, P.; Sofokleous, P.; Humphrey, E.; Locke, I.; Edirisinghe, M.; Terracciano, C.; Boccaccini, A. R.; Knowles, J. C.; Harding, S. E.; Roy, I. Poly(3-hydroxyoctanoate), a promising new material for cardiac tissue engineering. *J. Tissue Eng. Regener. Med.* **2018**, *12*, e495−e512.

(22) Garcia-Garcia, D.; Rayón, E.; Carbonell-Verdu, A.; Lopez-Martinez, J.; Balart, R. Improvement of the compatibility between poly(3-hydroxybutyrate) and poly(ε-caprolactone) by reactive extrusion with dicumyl peroxide. *Eur. Polym. J.* **2017**, *86*, 41−57.

(23) Bucci, D. Z.; Tavares, L. B. B.; Sell, I. Biodegradation and physical evaluation of PHB packaging. *Polym. Testing* **2007**, *26*, 908−915.

(24) Koller, M. Poly(hydroxyalkanoates) for Food Packaging: Application and Attempts towards Implementation. *Appl. Food Biotechnol.* **2014**, *1*, No. 13.

(25) Misra, S. K.; Nazhat, S. N.; Valappil, S. P.; Moshrefi-Torbati, M.; Wood, R. J. K.; Roy, I.; Boccaccini, A. R. Fabrication and Characterization of Biodegradable Poly(3-hydroxybutyrate) Composite Containing Bioglass. *Biomacromolecules* **2007**, *8*, 2112−2119.

(26) Misra, S. K.; Mohn, D.; Brunner, T. J.; Stark, W. J.; Philip, S. E.; Roy, I.; Salih, V.; Knowles, J. C.; Boccaccini, A. R. Comparison of nanoscale and microscale bioactive glass on the properties of P(3HB)/Bioglass composites. *Biomaterials* **2008**, *29*, 1750−1761.

(27) Hajiali, H.; Karbasi, S.; Hosseinalipour, M.; Rezaie, H. R. Preparation of a novel biodegradable nanocomposite scaffold based on poly (3-hydroxybutyrate)/bioglass nanoparticles for bone tissue engineering. *J. Mater. Sci.: Mater. Med.* **2010**, *21*, 2125−2132.

(28) Shishatskaya, E. I.; Khlusov, I. A.; Volova, T. G. A hybrid PHB−hydroxyapatite composite for biomedical application: production, in vitro and in vivo investigation. *J. Biomater. Sci., Polym. Ed.* **2006**, *17*, 481−498.

(29) Akaraonye, E.; Filip, J.; Safarikova, M.; Salih, V.; Keshavarz, T.; Knowles, J. C.; Roy, I. Composite scaffolds for cartilage tissue engineering based on natural polymers of bacterial origin, thermoplastic poly(3-hydroxybutyrate) and micro-fibrillated bacterial cellulose. *Polym. Int.* **2016**, *65*, 780−791.

(30) Kim, H.; Abdala, A. A.; Macosko, C. W. Graphene/Polymer Nanocomposites. *Macromolecules* **2010**, *43*, 6515−6530.

(31) Potts, J. R.; Dreyer, D. R.; Bielawski, C. W.; Ruoff, R. S. Graphene-based polymer nanocomposites. *Polymer* **2011**, *52*, 5−25.

DOI: 10.1021/acsomega.9b02528
ACS Omega 2019, 4, 19746−19755

(32) Papageorgiou, D. G.; Kinloch, I. A.; Young, R. J. Mechanical properties of graphene and graphene-based nanocomposites. *Prog. Mater. Sci.* **2017**, *90*, 75−127.
(33) Gatti, T.; Vicentini, N.; Mba, M.; Menna, E. Organic Functionalized Carbon Nanostructures for Functional Polymer-Based Nanocomposites. *Eur. J. Org. Chem.* **2016**, *2016*, 1071−1090.
(34) Xu, C.; Jia, Z.; Wu, D.; Han, Q.; Meek, T. Fabrication of nylon-6/carbon nanotube composites. *J. Electron. Mater.* **2006**, *35*, 954−957.
(35) Lee, W.; Kang, Y. H.; Lee, J. Y.; Jang, K.-S.; Cho, S. Y. Hot-pressing for improving performance of CNT/conjugated polymer thermoelectric films and power generators. *Mater. Today Commun.* **2017**, *10*, 41−45.
(36) Cataldi, P.; Ceseracciu, L.; Marras, S.; Athanassiou, A.; Bayer, I. S. Electrical conductivity enhancement in thermoplastic polyurethane-graphene nanoplatelet composites by stretch-release cycles. *Appl. Phys. Lett.* **2017**, *110*, No. 121904.
(37) Cataldi, P.; Bayer, I. S.; Nanni, G.; Athanassiou, A.; Bonaccorso, F.; Pellegrini, V.; del Rio Castillo, A. E.; Ricciardella, F.; Artyukhin, S.; Tronche, M.-A.; Gogotsi, Y.; Cingolani, R. Effect of graphene nanoplatelet morphology on the elastic modulus of soft and hard biopolymers. *Carbon* **2016**, *109*, 331−339.
(38) Papadopoulou, E. L.; Paul, U. C.; Tran, T. N.; Suarato, G.; Ceseracciu, L.; Marras, S.; d'Arcy, R.; Athanassiou, A. Sustainable Active Food Packaging from Poly(lactic acid) and Cocoa Bean Shells. *ACS Appl. Mater. Interfaces* **2019**, *11*, 31317−31327.
(39) Papadopoulou, E. L.; Pignatelli, F.; Marras, S.; Marini, L.; Davis, A.; Athanassiou, A.; Bayer, I. S. Nylon 6,6/graphene nanoplatelet composite films obtained from a new solvent. *RSC Adv.* **2016**, *6*, 6823−6831.
(40) Matharu, R. K.; Porwal, H.; Ciric, L.; Edirisinghe, M. he effect of graphene−poly(methyl methacrylate) fibres on microbial growth. *Interface Focus* **2018**, *8*, No. 20170058.
(41) Mahalingam, S.; Homer-Vanniasinkam, S.; Edirisinghe, M. Novel pressurised gyration device for making core-sheath polymer fibres. *Mater. Des.* **2019**, *178*, No. 107846.
(42) de Moraes, J. O.; Scheibe, A. S.; Sereno, A.; Laurindo, J. B. Scale-up of the production of cassava starch based films using tape-casting. *J. Food Eng.* **2013**, *119*, 800−808.
(43) Shojaeiarani, J.; Bajwa, D. S.; Rehovsky, C.; Bajwa, S. G.; Vahidi, G. Deterioration in the Physico-Mechanical and Thermal Properties of Biopolymers Due to Reprocessing. *Polymers* **2019**, *11*, No. 58.
(44) Higuchi-Takeuchi, M.; Morisaki, K.; Toyooka, K.; Numata, K. Synthesis of High-Molecular-Weight Polyhydroxyalkanoates by Marine Photosynthetic Purple Bacteria. *PLoS One* **2016**, *11*, No. e0160981.
(45) Mottin, A. C.; Ayres, E.; Oréfice, R. L.; Câmara, J. J. D. What Changes in Poly(3-Hydroxybutyrate) (PHB) When Processed as Electrospun Nanofibers or Thermo-Compression Molded Film? *Mater. Res.* **2016**, *19*, 57−66.
(46) Wang, C.; Hsu, C.-H.; Hwang, I. H. Scaling laws and internal structure for characterizing electrospun poly[(R)-3-hydroxybutyrate] fibers. *Polymer* **2008**, *49*, 4188−4195.
(47) Ghasemi, M.; Singapati, A. Y.; Tsianou, M.; Alexandridis, P. Dissolution of semicrystalline polymer fibers: Numerical modeling and parametric analysis. *AIChE J.* **2017**, *63*, 1368−1383.
(48) Zhang, J.; Qiu, Z. Morphology, Crystallization Behavior, and Dynamic Mechanical Properties of Biodegradable Poly(ε-caprolactone)/Thermally Reduced Graphene Nanocomposites. *Ind. Eng. Chem. Res.* **2011**, *50*, 13885−13891.
(49) Izumi, C. M. S.; Temperini, M. L. A. FT-Raman investigation of biodegradable polymers: Poly(3-hydroxybutyrate) and poly(3-hydroxybutyrate-co-3-hydroxyvalerate). *Vib. Spectrosc.* **2010**, *54*, 127−132.
(50) Khafagy, R. M. In situ FT-Raman spectroscopic study of the conformational changes occurring in isotactic polypropylene during its melting and crystallization processes. *J. Polym. Sci., Part B: Polym. Phys.* **2006**, *44*, 2173−2182.
(51) Ferrari, A. C.; Meyer, J. C.; Scardaci, V.; Casiraghi, C.; Lazzeri, M.; Mauri, F.; Piscanec, S.; Jiang, D.; Novoselov, K. S.; Roth, S.; Geim, A. K. Raman Spectrum of Graphene and Graphene Layers. *Phys. Rev. Lett.* **2006**, *97*, No. 187401.
(52) Mark, J. E. *Physical Properties of Polymers Handbook*; Springer, 2007.
(53) Irimia-Vladu, M.; Głowacki, E. D.; Voss, G.; Bauer, S.; Sariciftci, N. S. Green and biodegradable electronics. *Mater. Today* **2012**, *15*, 340−346.
(54) Misra, S. K.; Watts, P. C. P.; Valappil, S. P.; Silva, S. R. P.; Roy, I.; Boccaccini, A. R. Poly(3- hydroxybutyrate)/Bioglasscomposite films containing carbon nanotubes. *Nanotechnology* **2007**, *18*, No. 075701.
(55) Cataldi, P.; Bayer, I. S.; Bonaccorso, F.; Pellegrini, V.; Athanassiou, A.; Cingolani, R. Foldable Conductive Cellulose Fiber Networks Modified by Graphene Nanoplatelet-Bio-Based Composites. *Adv. Electron. Mater.* **2015**, *1*, No. 1500224.
(56) Schneider, Y.; Kluge, C.; Weiß, U.; Rohm, H. Chapter 12: Packaging Materials and Equipment. In *Technology of Cheesemaking*, 2nd Edition; Law, B. A.; Tamime, A. Y., Eds.; Wiley, 2010.
(57) Miguel, O.; Iruin, J. J. Evaluation of the transport properties of Poly(3-hydroxybutyrate) and its 3-hydroxyvalerate copolymers for packaging applications. *Macromol. Symp.* **1999**, *144*, 427−438.
(58) Martínez-Sanz, M.; Villano, M.; Oliveira, C.; Albuquerque, M. G. E.; Majone, M.; Reis, M.; Lopez-Rubio, A.; Lagaron, J. M. Characterization of polyhydroxyalkanoates synthesized from microbial mixed cultures and of their nanobiocomposites with bacterial cellulose nanowhiskers. *New Biotechnol.* **2014**, *31*, 364−376.
(59) Bai, H.; Huang, C.; Xiu, H.; Zhang, Q.; Deng, H.; Wang, K.; Chen, F.; Fu, Q. Significantly Improving Oxygen Barrier Properties of Polylactide via Constructing Parallel-Aligned Shish-Kebab-Like Crystals with Well-Interlocked Boundaries. *Biomacromolecules* **2014**, *15*, 1507−1514.
(60) Ahmed, J.; Mulla, M.; Arfat, Y. A.; Thai T, L. A. Mechanical, thermal, structural and barrier properties of crab shell chitosan/graphene oxide composite films. *Food Hydrocolloids* **2017**, *71*, 141−148.
(61) Pinto, A. M.; Cabral, J.; Tanaka, D. A. P.; Mendes, A. M.; Magalhães, F. D. Effect of incorporation of graphene oxide and graphene nanoplatelets on mechanical and gas permeability properties of poly(lactic acid) films. *Polym. Int.* **2013**, *62*, 33−40.
(62) Silva, T. F. d.; Menezes, F.; Montagna, L. S.; Lemes, A. P.; Passador, F. R. Preparation and characterization of antistatic packaging for electronic components based on poly(lactic acid)/carbon black composites. *J. Appl. Polym. Sci.* **2019**, *136*, No. 47273.
(63) Illyefalvi-Vitéz, Z. In *Graphene and Its Potential Applications in Electronics Packaging—A Review*, Proceedings of the 36th International Spring Seminar on Electronics Technology, 2013; pp 323−328.
(64) Chang, C.-H.; Huang, T.-C.; Peng, C.-W.; Yeh, T.-C.; Lu, H.-I.; Hung, W.-I.; Weng, C.-J.; Yang, T.-I.; Yeh, J.-M. Novel anticorrosion coatings prepared from polyaniline/graphene composites. *Carbon* **2012**, *50*, 5044−5051.
(65) Shim, S. H.; Kim, K. T.; Lee, J. U.; Jo, W. H. Facile Method to Functionalize Graphene Oxide and Its Application to Poly(ethylene terephthalate)/Graphene Composite. *ACS Appl. Mater. Interfaces* **2012**, *4*, 4184−4191.
(66) Al-Jabareen, A.; Al-Bustami, H.; Harel, H.; Marom, G. Improving the oxygen barrier properties of polyethylene terephthalate by graphite nanoplatelets. *J. Appl. Polym. Sci.* **2013**, *128*, 1534−1539.
(67) Arrieta, M.; Samper, M.; Aldas, M.; López, J. On the Use of PLA-PHB Blends for Sustainable Food Packaging Applications. *Materials* **2017**, *10*, No. 1008.
(68) Cui, Y.; Kundalwal, S. I.; Kumar, S. Gas barrier performance of graphene/polymer nanocomposites. *Carbon* **2016**, *98*, 313−333.
(69) Yokouchi, M.; Chatani, Y.; Tadokoro, H.; Teranishi, K.; Tani, H. Structural studies of polyesters: 5. Molecular and crystal structures of optically active and racemic poly (β-hydroxybutyrate). *Polymer* **1973**, *14*, 267−272.

DOI: 10.1021/acsomega.9b02528
ACS Omega 2019, 4, 19746−19755